JOURNAL OF SOLID STATE CHEMISTRY 29, 47–62 (1979)

Structural Aspects of the Metal-Insulator Transitions in $(Ti_{0.9975}V_{0.0025})_4O_7$

J. L. HODEAU AND M. MAREZIO

Laboratoire de Cristallographie, Centre National de la Recherche Scientifique, 166X-38042 Grenoble Cedex, France

Received May 16, 1978; in final form September 11, 1978

The structure of $(Ti_{0.9975}V_{0.0025})_4O_7$ has been refined at 298, 135, and 100°K from single-crystal X-ray diffraction data. This sample belongs to the region of the Ti_4O_7/V_4O_7 phase diagram where still two electrical transitions are observed. The three structures of the V-doped sample are almost identical to the corresponding structures of pure Ti_4O_7. The charges are disordered in the metallic phase, they order very slightly in the intermediate phase, and they are almost completely ordered along the 3113 and the 4224 chains in the low-temperature phase. There is no evidence of cation pair-bond formation in the intermediate phase, whereas the Ti^{3+} cations are all paired in the low-temperature phase. The cationic Debye–Waller factors in the intermediate phase are anomalously large, which is indicative of a disorder. Thus, in order to explain the physical properties of the intermediate phase, as in the case of the pure sample, all the Ti^{3+} cations are thought to form pair bonds with no long-range order. The Ti–Ti distances along the pseudorutile c-axis are shorter in the V-doped sample than in the pure one. This indicates that the relative bond strengths increase with the incorporation of vanadium. The main difference between pure Ti_4O_7 and $(Ti_{0.9975}V_{0.0025})_4O_7$ is in the lattice parameters and unit-cell volume variations with temperature. In the latter sample two discontinuities are observed, each corresponding to one transition, whereas in the former only one transition is observed, which corresponds to the higher transition. In the low-temperature phase the V cations are either 3+ or 4+ and are either on the 3113 chains or on the 4224 chains. The V doping gives rise to four different patterns. Each one is discussed in order to explain the differences between V-doped sample and pure Ti_4O_7.

Ti_4O_7 and V_4O_7 are isostructural and belong to the M_nO_{2n-1} homologous series. Since they are in the middle of the M_2O_3–MO_2 system they contain 3^+ and 4^+ cations in equal proportions. Their structure is derived from that of rutile in the sense that it consists of successive rutile blocks which are infinite in two dimensions and four octahedra long in the third. The two infinite dimensions are contained in the $(1\bar{2}1)$ plane of the pseudorutile lattice. Inside each rutile block the octahedra share edges and corners and form rutile octahedral chains. Along the $(1\bar{2}1)$ planes separating the blocks, the octahedra share faces, edges, and corners. These planes are usually called crystallographic shear planes. A schematic arrangement of the octahedra in these structures is shown in Fig. 1. It can be seen that if in one rutile block the octahedra, forming the chains along the pseudorutile c-axis, are centered on the (0 0 0) and $(\frac{1}{2}\frac{1}{2}\frac{1}{2})$ positions, in the adjacent block the octahedra are centered on the $(\frac{1}{2}\ 0\ 0)$ and $(0\ \frac{1}{2}\ \frac{1}{2})$ positions. The resulting structure is triclinic, space group $A\bar{1}$ [we use the cell proposed by Andersson and Jahnberg (*1*)], with four formulas per unit cell. The four crystallographic independent cation sites form two types of pseudorutile chains, such as M(3)–M(1)–M(1)–M(3) and

0022-4596/79/070047-16$02.00/0
Copyright © 1979 by Academic Press, Inc.
All rights of reproduction in any form reserved.
Printed in Great Britain

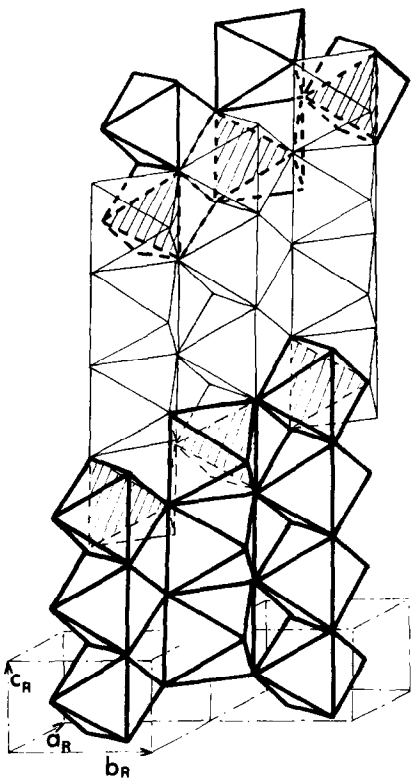

FIG. 1. The stacking of the oxygen octahedra containing titanium in each rutile block of Ti_4O_7 structure. Successive rutile blocks are represented by heavy and light lines; (a_R, b_R, c_R) represent the pseudorutile cell parameters; shaded octahedra faces are common faces between 3113 and 4224 chains in the $(1\bar{2}1)$ shear plane.

M(4)–M(2)–M(2)–M(4), which we refer to as 3113 and 4224.

Ti_4O_7 exhibits two electrical transitions: a semiconductor–semiconductor transition at 130°K (lower transition) and a second from a semiconducting to a metallic state at 150°K (higher transition). The magnetic susceptibility, the lattice parameters, and the unit-cell volume show discontinuities only at the latter transition. The crystal structures of the three different phases (low-temperature, intermediate, and metallic phases) indicated that in the metallic phase the Ti cations have an average effective charge of ~3.5, while in the low-temperature phase the electrons are localized into alternate chains of 3^+ and 4^+ cations along the pseudorutile c-axis. The Ti^{3+} and Ti^{4+} cations are situated along the 3113 and 4224 chains, respectively. Furthermore, covalent metal–metal bonds form between adjacent Ti^{3+} cations. The schematization of the bonding pattern is 3–1 . . . 1–3, 4 . . . 2 . . . 2 . . . 4 The intermediate phase is characterized by the same charge localization and pair-bond formation as the low-temperature phase; however, no long-range correlation exists in the intermediate phase. The lower transition is then viewed as an order–disorder one. Heat capacity and EPR measurements showed that this disorder is dynamic and at the unit-cell level (*2*).

The physical properties of V_4O_7 are relatively different (*3*). It exhibits also two transitions; however, the first, at 40°K is from an antiferromagnetic to a paramagnetic state. The second, at 250°K, is from a semiconducting to a metallic state. This latter state is characterized by a disorder of the V^{3+} and V^{4+} cations over the four independent sites and by one pair bond V(1)–V(1) along the 3113 chains. Below the 250°K transition the semiconducting phase of V_4O_7 is characterized by a separation of charges into alternate chains of V^{3+} and V^{4+} sites running along the pseudorutile c-axis and by the formation of two more metal–metal pair bonds. The V^{3+} and V^{4+} cations are found to be on the 4224 and 3113 chains, respectively. The bonding pattern is 3 . . . 1–1 . . . 3, 4–2 . . . 2–4, which is different from that found in Ti_4O_7. The unpaired V^{4+} on the (3) site would contribute to the antiferromagnetic order which takes place at 40°K.

It has been shown that the incorporation of vanadium into Ti_4O_7 changes the physical properties of this compound (*4*). Figure 2 shows the phase diagram of the $(Ti_{1-x}V_x)_4O_7$ system for $x < 1.7\%$ as determined by calorimetric measurements (*5*). The two transitions still exists for $x < \sim 0.4\%$; however, the two temperatures are found to be lower, with the 130°K transition decreasing

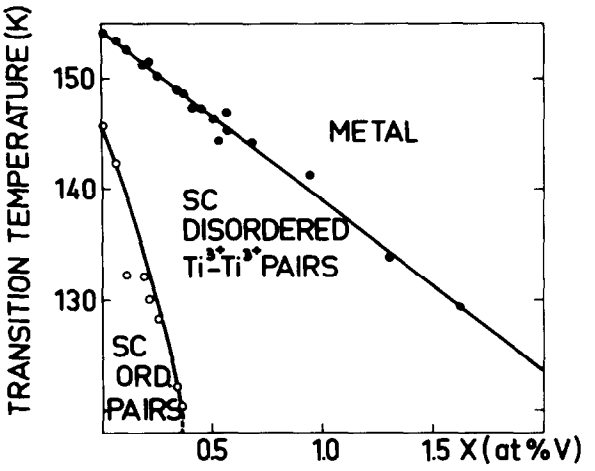

FIG. 2. Phase diagram showing transition temperatures between low-temperature and intermediate semiconducting phases and between intermediate and high-temperature metallic phases versus vanadium concentration x (*5*).

much faster than the 150°K transition. Electrical resistivity measurements down to 4°K show that the former disappears for $x > \sim 0.6\%$, while the latter continues to decrease with increasing x. For instance, at $x = 1.7\%$ the semiconductor-to-metal transition temperature has decreased 130°K.

This paper reports the determination of the crystal structure of $(Ti_{0.9975}V_{0.0025})_4O_7$ at 298, 135, and 100°K, along with the lattice parameter variation between room temperature and 90°K. These results are compared with those of pure Ti_4O_7 (*6*) and of $(Ti_{0.994}V_{0.006})_4O_7$. This latter compound belongs to the region of the phase diagram where the order–disorder transition has been suppressed.

Crystal Data

Single crystals of $(Ti_{-x}V_x)_4O_7$ were grown by chemical transport reaction. The proper stoichiometric amounts of Ti_3O_5 and V_4O_7 powders were mixed, pressed, and fired at 2000°C in an argon atmosphere in order to prepare the $(T_{1-x}V_x)_3O_5$ powder which was used as the starting material together with $TeCl_4$ as the transport agent. The details of the crystal preparations have been published elsewhere (*7*). Precession photographs showed that the crystals obtained consisted of a single phase and were isostructural with Ti_4O_7. The vanadium content was determined by atomic absorption analysis with an accuracy of $\simeq 10\%$. All V-doped crystals have been found to be twinned according to the laws described in Ref. (*8*). However, the crystal of $(Ti_{0.9975}V_{0.0025})_4O_7$ used in the intensity data collection was a single individual because the other twinned individuals were eliminated during the grinding procedure. This sphere ($R = 0.139(4)$ mm) was mounted on an automatic Philips X-ray diffractometer equipped with a graphite monochromator and Ag$K\alpha$ radiation. The low temperatures were attained by blowing a cold stream of nitrogen directly onto the crystal. A control unit was used to monitor the temperature and the proper gas flow.

For the determination of the lattice parameter variations with temperature, the θ angle of 25 reflections controlling the orientation matrix were used. They are chosen in the region where a complete α_1/a_2 separation occurred. The final values were given by the refinement program of the Philips software. At the temperatures at which the intensity data collections were carried out,

namely 298, 135, and 100°K, the lattice parameters were determined on cooling and on warming by the use of the θ angles of 19 independent reflections measured in the region $53° < 2\theta < 61°$. The zero of the θ circle was determined for each of 19 reflections by measuring the θ and $-\theta$ values. The final values obtained by the use of the PARAM refinement program are given in Table I. Figure 3 shows the variation of the lattice parameters and unit-cell volume as a function of temperature. The values obtained from the orientation matrix have been scaled to the values reported in Table I. The variations of the lattice parameters for pure Ti_4O_7 (9) are outlined for comparison.

The integrated intensities were obtained by the use of the ω-scan technique, and the background was collected at $\sim \pm 0.7°$ off the peak maximum. At room temperature 8466 reflections included in the interval $4° < 2\theta < 80°$, at 135°K 2188 independent reflections in $4° < 2\theta < 60°$, and at 100°K 4689 reflections in $4° < 2\theta < 60°$ were measured. In order to check the sample orientation and the beam stability three well-defined standard reflections were measured about every 2 hr. For some reflections the sample eccentricity was magnified, due to the ice formation at 100°K. This was detected because the two backgrounds, at each side of the peak, were not the same. Therefore those reflections were eliminated (and 4300 reflections were used for the refinement) for which

$$|I_{BGL} - I_{BGR}| > 4[(I_{BGL} + I_{BGR})/2]^{1/2}$$

or

$$|I_c - I_o|/I_m > 0.05\%.$$

I_{BGL}, I_{BGR} Left and right background intensities per unit time;

I_o $I - (I_{BGL} + I_{BGR})/2$ (observed intensity);

I Peak intensity per unit time;

I_M Highest observed intensity of the measurements at 100°K (0.05% I_M is approximatively the average value of I_{BGL} and I_{BGR});

I_c Intensity calculated with $I_{BGL} = I_{BGR} = \min(I_{BGL}, I_{BGR})$.

The intensities of the $(\bar{1}33)$, $(\bar{3}3\bar{1})$, and (231) reflections which were found to be very sensitive to the temperature variation and to have an abrupt change at the transition were used as indicators of the temperature and the transition. The intensities of these three reflections have similar variations with temperature, and therefore only one is shown in Fig. 4.

Refinements

The Lorentz, polarization, and absorption corrections ($\mu R = 0.483$) were applied in order to convert the integrated intensities

TABLE I

LATTICE PARAMETERS AND UNIT-CELL VOLUME ON COOLING AND ON WARMING AT 298, 135, AND 100°K

	298°K	135°K	100°K	135°K	298°K
a	5.5942(6)	5.5943(5)	5.6235(3)	5.5944(3)	5.5935(5)
b	7.1216(8)	7.1297(7)	7.1984(4)	7.1291(4)	7.1225(6)
c	12.460(1)	12.484(1)	12.4018(5)	12.4856(6)	12.4615(9)
α	95.05(1)	95.00(1)	95.056(7)	94.984(8)	95.07(1)
β	95.19(1)	95.426(9)	95.550(5)	95.422(5)	95.175(8)
γ	108.76(1)	109.023(9)	109.676(5)	109.018(6)	108.751(8)
V	464.48	464.93	466.58	465.00	464.56

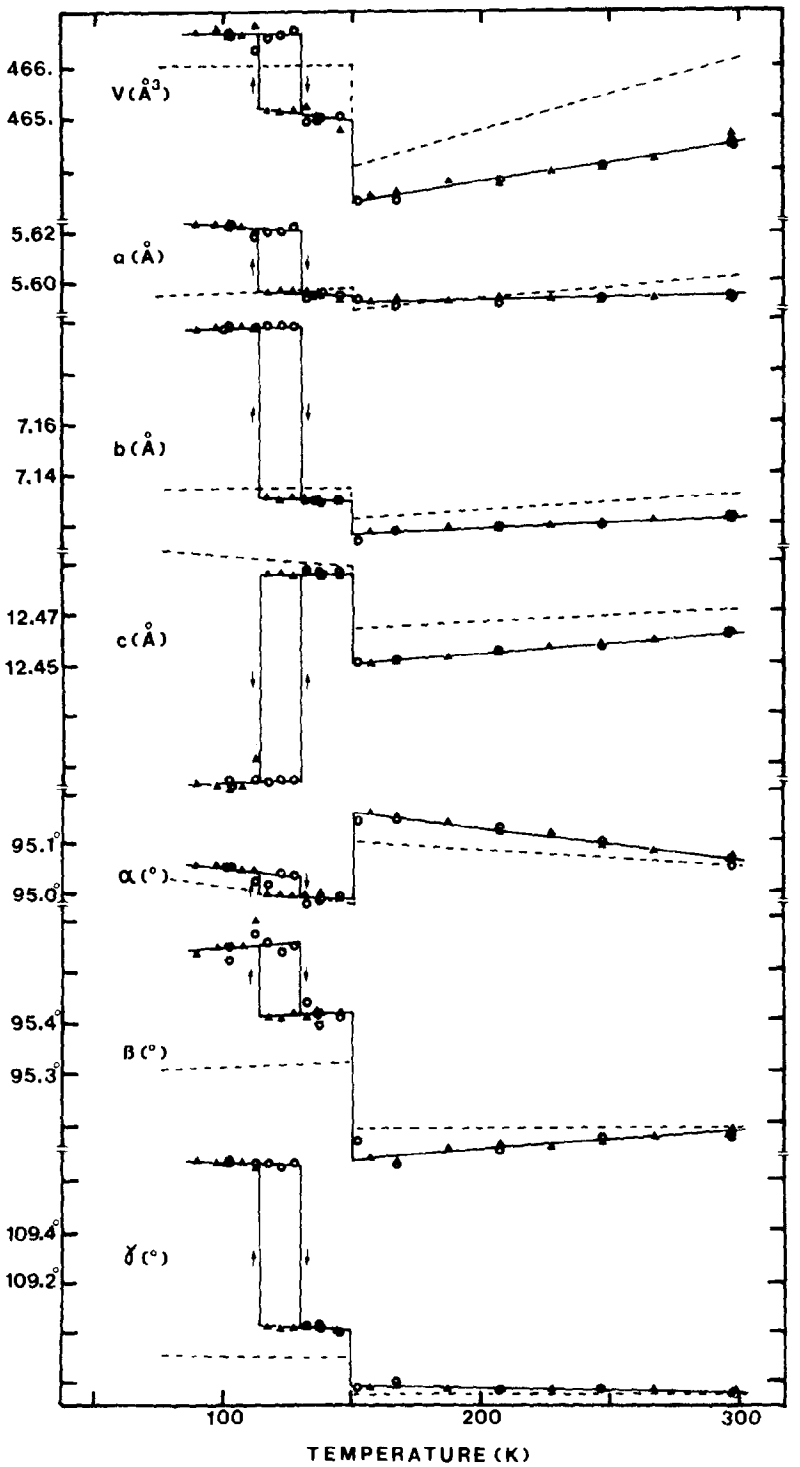

FIG. 3. Lattice parameters and unit-cell volume of $(Ti_{0.9975}V_{0.0025})_4O_7$ vs temperature. The solid triangles correspond to values measured on cooling and the circles, to values measured on warming. The variations of the lattice parameters for pure Ti_4O_7 are outlined.

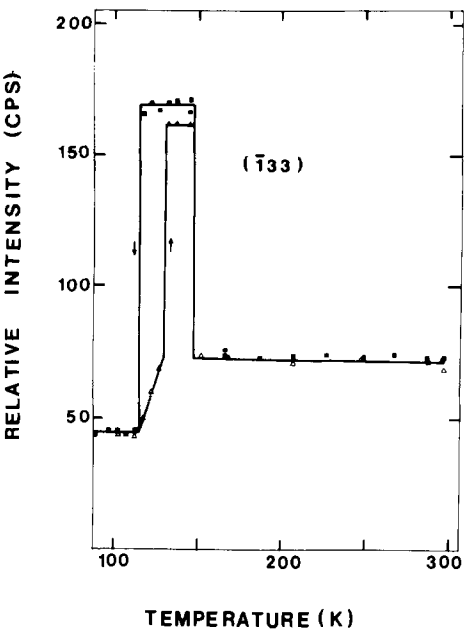

FIG. 4. Net intensity of ($\bar{1}33$) reflection of 0.25% V-doped Ti_4O_7 single crystal vs temperature. The solid squares represent values measured on cooling and the triangles represent values measured on warming.

into structure factors. The structures were refined with the assumption that the space group was $A\bar{1}$, which had been confirmed previously (*6*). The total numbers of independent reflections were 4430, 2188, and 2522 for 298, 135, and 100°K, respectively. For the three refinements the starting values for the positional and thermal parameters were those reported in Ref. (*6*). The form-factor tables for neutral atoms given by Doyle and Turner (*10*) were used, together with the f' and f'' values of titanium for AgK_α, reported by Cromer and Liberman (*11*). The LINEX refinement program was used. The reflections were weighted according to: $w = 1/\sigma^2(F)$, $\sigma(F)$ = quadratic deviation. In the final cycles of the refinements, 33 positional and 66 anisotropic thermal parameters and the isotropic type I secondary extinction factor were varied. The final wR and R factors were 0.048 and 0.025, 0.067 and 0.031, and 0.024 and 0.022 at 298, 135, and 100°K, respectively. The final positional and thermal parameters, the Lorentzian mosaic dispersion g are listed in Table II and III for the three temperatures. These values along with the lattice parameters given in the first, second, and third columns of Table I were used as input to the program BONDLA in order to calculate the interatomic distances and the thermal

TABLE II

POSITIONAL PARAMETERS OF 0.25% V-DOPED Ti_4O_7 AT 298, 135, AND 100°K

	298°K	135°K	100°K
Ti(1)x	0.21608(4)	0.21736(9)	0.23627(6)
y	0.15277(3)	0.15555(7)	0.16307(5)
z	0.06277(2)	0.06404(3)	0.06822(3)
Ti(2)x	0.21852(4)	0.21720(8)	0.21306(6)
y	0.65265(4)	0.65514(7)	0.67121(5)
z	0.06621(2)	0.06595(3)	0.06565(3)
Ti(3)x	0.68355(4)	0.68133(8)	0.66984(6)
y	0.44001(3)	0.44247(7)	0.43872(5)
z	0.20118(2)	0.20064(4)	0.19383(3)
Ti(4)x	0.68834(4)	0.68747(8)	0.70556(6)
y	0.94242(3)	0.94245(7)	0.94939(5)
z	0.20132(2)	0.19977(4)	0.20431(3)
O(1)x	0.1077(2)	0.1085(4)	0.1079(3)
y	0.8629(2)	0.8615(3)	0.8615(2)
z	0.0152(1)	0.0159(2)	0.0168(1)
O(2)x	0.5868(2)	0.5862(4)	0.5799(3)
y	0.7926(2)	0.7938(3)	0.7970(2)
z	0.0581(1)	0.0569(2)	0.0620(1)
O(3)x	0.8560(2)	0.8536(4)	0.8570(3)
y	0.4963(2)	0.4968(3)	0.4966(2)
z	0.0814(1)	0.0798(2)	0.0744(1)
O(4)x	0.3285(2)	0.3238(4)	0.3160(3)
y	0.4385(1)	0.4397(3)	0.4448(2)
z	0.1387(1)	0.1396(2)	0.1419(1)
O(5)x	0.5261(2)	0.5271(4)	0.5278(3)
y	0.1449(1)	0.1436(3)	0.1364(2)
z	0.1639(1)	0.1654(2)	0.1688(1)
O(6)x	0.0379(2)	0.0398(4)	0.0373(3)
y	0.0708(2)	0.0708(3)	0.0709(2)
z	0.1984(1)	0.1978(2)	0.1977(1)
O(7)x	0.2950(2)	0.2909(4)	0.2846(3)
y	0.7902(1)	0.7856(3)	0.7796(2)
z	0.2237(1)	0.2234(2)	0.2226(1)

TABLE III

THERMAL PARAMETERS ($\times 10^4$) AND LORENTZIAN MOSAIC DISPERSION g OF 0.25% V-DOPED Ti_4O_7[a]

	298°K	135°K	100°K
Ti(1)β_{11}	37.1(5)	46(2)	26.7(9)
β_{22}	21.4(3)	16(1)	12.7(6)
β_{33}	6.4(1)	5.6(3)	3.7(2)
β_{12}	9.9(3)	12.4(8)	6.9(6)
β_{13}	0.5(2)	6.3(4)	1.4(3)
β_{23}	1.1(1)	1.7(3)	0.4(2)
Ti(2)β_{11}	35.4	39	22.7
β_{22}	21.1	19	13.6
β_{33}	6.2	4.1	4.3
β_{12}	8.9	7.7	4.9
β_{13}	1.1	2.1	0.4
β_{23}	1.4	2.1	0.9
Ti(3)β_{11}	37.5	34	23.1
β_{22}	19.7	17	13.5
β_{33}	6.8	9.2	4.1
β_{12}	9.7	10.6	5.6
β_{13}	3.8	7.5	2.5
β_{23}	1.8	4.7	1.2
Ti(4)β_{11}	38.6	44	21.4
β_{22}	21.6	15	13.7
β_{33}	7.4	5.3	4.2
β_{12}	12.0	13.7	5.3
β_{13}	4.2	2.6	1.4
β_{23}	2.9	2.7	0.9
O(1)β_{11}	49(2)	45(4)	41(4)
β_{22}	24(1)	26(3)	18(2)
β_{33}	10.3(3)	12(1)	6.8(7)
β_{12}	15(1)	18(3)	12(2)
β_{13}	−1.1(6)	0(2)	0(1)
β_{23}	3.1(5)	5(1)	−0(1)
O(2)β_{11}	43	31	30
β_{22}	31	21	21
β_{33}	8.6	11	5.6
β_{12}	6	5	6
β_{13}	5.8	−3	3
β_{23}	1.4	3	−0
O(3)β_{11}	49	23	29
β_{22}	34	31	19
β_{33}	7.6	10	5.6
β_{12}	9	1	5
β_{13}	5.6	3	4
β_{23}	1.8	2	0
O(4)β_{11}	44	43	38
β_{22}	22	15	18
β_{33}	8.3	7	5.6
β_{12}	14	9	12
β_{13}	−0.3	3	1
β_{23}	1.1	5	0
O(5)β_{11}	38	34	34
β_{22}	23	23	16
β_{33}	7.1	8	5.8
β_{12}	12	6	8
β_{13}	1.3	−4	3
β_{23}	1.8	1	1
O(6)β_{11}	31	24	33
β_{22}	34	13	22
β_{33}	7.2	8	5.4
β_{12}	8	3	8
β_{13}	2.4	2	2
β_{23}	4.8	3	2
O(7)β_{11}	44	34	33
β_{22}	22	8	16
β_{33}	6.9	7	6.5
β_{12}	10	−2	8
β_{13}	0.8	−1	3
β_{23}	1.4	3	1
g	69″	113″	126″

[a] In this table the standard deviations for all titanium and all oxygen thermal parameters are the same as those for Ti(1) and O(1), respectively.

data with their standard deviations. These values are reported in Tables IV, V, and VI, respectively. For comparison in Table VI we report the mean values of the root-mean-square displacements (RMSD) for all the atoms along with the relative standard deviations. These values do not have a precise physical meaning; however, they give an idea of the evolution with temperature of the thermal vibrations. The values of a previous study of pure Ti_4O (*6*) are listed for comparison.

The cation charges are given in Table VII. They were calculated by the empirical formula deduced by Zachariasen (*12*) which takes into account the distortion of coordination polyhedron: $d = d(1) \times (1 - 0.171 \ln S)$; S and d are the bond strength and the distance between two atoms, and

TABLE IV

Ti–Ti DISTANCES (Å) OF PURE Ti_4O_7(6) AND 0.25% V-DOPED Ti_4O_7[a]

	Ti_4O_7			$(Ti_{0.9975}V_{0.0025})_4O_7$		
	298°K	140°K	120°K	298°K	135°K	100°K
Ti(1)–Ti(1)e	2.895(1)	2.926(2)	3.133(2)	2.8912(5)	2.9190(9)	3.1089(7)
–Ti(3)e	3.020(1)	2.990(2)	2.802(2)	3.0198(3)	2.9871(5)	2.7877(4)
–Ti(2)c	3.604(1)	3.609(1)	3.550(2)	3.6055(3)	3.6097(6)	3.5531(5)
–Ti(2)c	3.502(1)	3.491(1)	3.461(1)	3.5023(4)	3.4842(7)	3.4830(5)
–Ti(2)c	3.572(1)	3.574(3)	3.465(3)	3.5703(4)	3.5698(7)	3.4960(5)
–Ti(2)c	3.553(1)	3.554(3)	3.671(3)	3.5522(4)	3.5604(7)	3.7066(5)
–Ti(4)c	3.793(1)	3.783(2)	3,784(2)	3.7920(4)	3.7824(8)	3.8090(6)
–Ti(4)c	3.530(1)	3.526(2)	3.534(2)	3.5317(3)	3.5255(6)	3.5302(5)
–Ti(4)c	3.425(1)	3.434(2)	3.498(2)	3.4252(4)	3.4338(6)	3.4779(5)
–Ti(3)er	3.111(1)	3.124(2)	3.159(2)	3.1120(4)	3.1211(7)	3.1408(5)
–Ti(4)cr	3.806(1)	3.795(2)	3.699(2)	3.8039(3)	3.7985(6)	3.6969(5)
Ti(2)–Ti(2)e	2.942(1)	2.937(2)	3.023(2)	2.9404(5)	2.9350(9)	3.0049(7)
–Ti(4)e	3.019(1)	3.000(2)	3.083(2)	3.0165(3)	2.9945(5)	3.0618(4)
–Ti(3)c	3.751(1)	3.746(2)	3.778(1)	3.7523(4)	3.7487(7)	3.8079(6)
–Ti(3)c	3.538(1)	3.539(2)	3.557(1)	3.5386(3)	3.5422(6)	3.5532(5)
–Ti(3)c	3.464(1)	3.473(2)	3.439(2)	3.4657(4)	3.4776(6)	3.4245(5)
–Ti(4)er	3.067(1)	3.101(2)	3.104(1)	3.0691(4)	3.1023(7)	3.0909(5)
–Ti(3)cr	3.788(1)	3.773(2)	3.765(2)	3.7850(3)	3.7700(6)	3.7569(5)
Ti(3)–Ti(4)c	3.556(1)	3.573(2)	3.576(2)	3.5527(3)	3.5756(7)	3.6079(5)
–Ti(4)c	3.569(1)	3.555(2)	3.568(2)	3.5695(3)	3.5548(7)	3.6033(5)
–Ti(4)fr	2.811(1)	2.806(1)	2.838(1)	2.8113(4)	2.8082(7)	2.8605(6)
–Ti(4)cr	3.417(1)	3.434(1)	3.414(1)	3.4174(3)	3.4336(6)	3.4116(5)
–Ti(3)er	3.237(1)	3.261(2)	3.267(1)	3.2372(5)	3.2558(10)	3.2648(7)
Ti(4)–Ti(4)er	3.280(1)	3.295(2)	3.389(2)	3.2798(5)	3.2937(10)	3.3883(7)
Ti(1)–Ti(1)e, Ti(1)–Ti(3)e average	2.958	2.958	2.968	2.9555	2.9531	2.9483
Ti(2)–Ti(2)e, Ti(2)–Ti(4)e average	2.981	2.969	3.053	2.9785	2.9648	3.0334
	Distance variations from room temperature of					
Ti(1)–Ti(1)e	0.0	0.031	0.238	0.0	0.0278	0.2177
Ti(1)–Ti(3)e	0.0	−0.030	−0.218	0.0	−0.0327	−0.2321
Ti(2)–Ti(2)e	0.0	−0.005	0.081	0.0	−0.0054	0.0645
Ti(2)–Ti(4)e	0.0	−0.019	0.064	0.0	−0.0220	0.0453

[a] The symbols c, e, and f refer to Ti–Ti distances across a shared octahedral corner, edge, or face, respectively. Symbol r indicates Ti–Ti distances between rutile blocks.

$d(1)$ is the distance corresponding to unit-bond strength. The $d(1)$ value (1.830 Å) for Ti–O was calculated from the charges and Ti–O distances at room temperature of:

TiO_2	Abrahams and Bernstein (*13*) $d(1) = 1.8317$
Ti_2O_3	Robinson (*14*) $d(1) = 1.8300$

TABLE V

INTERATOMIC DISTANCES (Å) IN Ti–O OCTAHEDRA IN 0.25% V-DOPED Ti_4O_7

	298°K	135°K	100°K
Ti(1)–O(1)	1.941(1)	1.955(2)	2.057(2)
–O(1)	1.974(1)	2.002(2)	2.062(1)
–O(2)	1.940(1)	1.941(2)	1.991(1)
–O(4)	2.040(1)	2.031(2)	2.033(1)
–O(5)	2.068(1)	2.076(2)	2.035(2)
–O(6)	2.073(1)	2.059(2)	2.075(1)
Average	2.006	2.011	2.042
Average in pure Ti_4O_7(6)	2.006	2.011	2.043
O(5)–O(6)e(1/3)	2.692(1)	2.681(3)	2.703(2)
O(5)–O(4)e(1/3)	2.689(2)	2.733(3)	2.880(2)
O(5)–O(2)	2.886(1)	2.893(3)	2.982(2)
O(5)–O(1)	2.912(1)	2.909(2)	2.895(2)
O(1)–O(6)	2.837(1)	2.847(3)	2.838(2)
O(1)–O(4)	3.049(1)	3.038(2)	3.034(2)
O(1)–O(2)	2.901(2)	2.905(3)	2.964(2)
O(1)–O(1)e(1/1)	2.640(2)	2.672(4)	2.702(3)
O(2)–O(4)	2.992(1)	3.018(3)	3.157(2)
O(2)–O(1)	2.785(1)	2.780(3)	2.816(2)
O(6)–O(4)	2.806(1)	2.792(3)	2.807(2)
O(6)–O(1)	2.738(2)	2.735(3)	2.728(2)
Average	2.827	2.834	2.876
Standard deviation	0.126	0.122	0.140
Average in pure Ti_4O_7(6)	2.827	2.834	2.876
Standard deviation	0.125	0.122	0.159
Ti(2)–O(1)	1.930(1)	1.896(2)	1.793(2)
–O(2)	1.995(1)	1.996(2)	1.961(2)
–O(3)	2.011(1)	2.011(2)	1.993(1)
–O(3)	1.978(1)	1.970(2)	1.952(1)
–O(4)	2.066(1)	2.074(2)	2.165(2)
–O(7)	2.057(1)	2.044(2)	1.982(1)
Average	2.006	1.999	1.974
Average in pure Ti_4O_7(6)	2.006	2.000	1.973
O(7)–O(1)	2.865(1)	2.855(3)	2.832(2)
O(7)–O(2)e(2/4)	2.742(1)	2.768(3)	2.699(2)
O(7)–O(3)	2.968(1)	2.946(2)	2.915(2)
O(7)–O(4)e(2/4)	2.702(2)	2.663(3)	2.595(2)
O(3)–O(1)	2.805(2)	2.805(3)	2.799(2)
O(3)–O(2)	2.950(1)	2.920(2)	2.904(2)
O(3)–O(3)e(2/2)	2.696(2)	2.690(4)	2.555(3)
O(3)–O(4)	2.971(1)	2.947(3)	2.879(2)
O(3)–O(1)	2.776(1)	2.755(3)	2.726(2)
O(3)–O(4)	2.842(2)	2.832(3)	2.790(2)
O(2)–O(1)	2.893(2)	2.874(3)	2.857(2)
O(2)–O(4)	2.797(1)	2.814(3)	2.794(2)

TABLE V—*continued*

	298°K	135°K	100°K
Average	2.834	2.822	2.779
Standard deviation	0.098	0.093	0.116
Average in pure Ti_4O_7(6)	2.834	2.824	2.776
Standard deviation	0.097	0.097	0.126
Ti(3)–O(5)	2.155(1)	2.148(2)	2.134(1)
–O(6)	1.934(1)	1.948(2)	2.047(2)
–O(7)	2.024(1)	2.034(2)	2.116(1)
–O(5)	1.993(1)	2.011(2)	2.033(1)
–O(4)	2.063(1)	2.065(2)	2.048(2)
–O(3)	1.854(1)	1.868(2)	1.895(2)
Average	2.004	2.012	2.046
Average in pure Ti_4O_7(6)	2.004	2.015	2.044
O(6)–O(5)e(3/1)	2.692(1)	2.681(3)	2.703(2)
O(6)–O(7)	2.835(2)	2.846(3)	2.902(2)
O(6)–O(5)	2.906(1)	2.886(2)	2.880(2)
O(6)–O(3)	2.868(1)	2.899(3)	2.948(2)
O(4)–O(5)f(3/4)	2.696(1)	2.677(3)	2.610(2)
O(4)–O(7)f(3/4)	2.693(1)	2.715(2)	2.736(2)
O(4)–O(5)e(1/3)	2.689(2)	2.733(3)	2.880(2)
O(4)–O(3)	3.007(2)	3.032(3)	3.144(2)
O(5)–O(7)f(3/4)	2.648(1)	2.663(3)	2.651(2)
O(5)–O(5)e(3/3)	2.599(2)	2.592(4)	2.591(3)
O(3)–O(7)	3.078(2)	3.103(3)	3.179(2)
O(3)–O(5)	2.924(1)	2.943(3)	3.040(2)
Average	2.803	2.814	2.855
Standard deviation	0.154	0.161	0.201
Average in pure Ti_4O_7(6)	2.804	2.816	2.853
Standard deviation	0.154	0.162	0.202
Ti(4)–O(4)	2.118(1)	2.120(2)	2.020(1)
–O(2)	1.933(1)	1.927(2)	1.927(1)
–O(7)	1.996(1)	1.989(2)	1.964(2)
–O(7)	2.173(1)	2.196(2)	2.314(1)
–O(6)	1.879(1)	1.887(2)	1.787(2)
–O(5)	2.001(1)	1.980(2)	1.983(2)
Average	2.017	2.017	1.999
Average in pure Ti_4O_7(6)	2.018	2.012	1.996
O(4)–O(7)e(2/4)	2.702(2)	2.663(3)	2.595(2)
O(4)–O(7)f(3/4)	2.693(1)	2.715(2)	2.736(2)
O(4)–O(6)	3.002(2)	2.995(3)	2.927(2)
O(4)–O(5)f(3/4)	2.696(1)	2.677(3)	2.610(2)
O(2)–O(7)	2.896(1)	2.913(3)	2.858(2)
O(2)–O(7)e(2/4)	2.742(1)	2.768(3)	2.699(2)
O(2)–O(6)	2.954(1)	2.952(2)	2.915(2)
O(2)–O(5)	2.863(2)	2.863(3)	2.792(2)

TABLE V—*continued*

	298°K	135°K	100°K
O(7)–O(7)e(4/4)	2.580(2)	2.590(4)	2.634(3)
O(7)–O(5)f(3/4)	2.648(1)	2.663(3)	2.651(2)
O(6)–O(7)	2.951(1)	2.926(3)	2.886(2)
O(6)–O(5)	3.074(2)	3.074(3)	3.050(2)
Average	2.817	2.817	2.779
Standard deviation	0.159	0.157	0.148
Average in pure Ti_4O_7(6)	2.818	2.811	2.775
Standard deviation	0.158	0.159	0.151

TABLE VI

ROOT-MEAN-SQUARE VALUES IN PURE Ti_4O_7(6) AND 0.25% V-DOPED Ti_4O_7[a]

	Ti_4O_7			$(Ti_{0.9975}V_{0.0025})_4O_7$		
	298°K	140°K	120°K	298°K	135°K	100°K
Ti(1)r_1	0.074	0.063	0.029	0.068	0.055	0.051
r_2	0.074	0.074	0.061	0.069	0.060	0.055
r_3	0.079	0.095	0.078	0.075	0.083	0.061
Ti(2)r_1	0.072	0.065	0.042	0.068	0.055	0.054
r_2	0.074	0.080	0.068	0.069	0.066	0.057
r_3	0.076	0.090	0.072	0.072	0.075	0.061
Ti(3)r_1	0.066	0.066	0.037	0.066	0.056	0.052
r_2	0.070	0.083	0.058	0.068	0.061	0.056
r_3	0.084	0.098	0.076	0.076	0.089	0.060
Ti(4)r_1	0.072	0.066	0.046	0.067	0.049	0.054
r_2	0.074	0.074	0.061	0.069	0.065	0.056
r_3	0.084	0.092	0.069	0.079	0.079	0.057
Mean value of RMS displacements of titanium atoms						
	0.075	0.079	0.058	0.071	0.066	0.056
Standard deviation with respect to the RMSD value						
	0.005	0.013	0.016	0.004	0.013	0.003
O(1)r_1	0.083	0.081	0.046	0.067	0.062	0.060
r_2	0.085	0.100	0.083	0.081	0.084	0.070
r_3	0.092	0.124	0.107	0.095	0.097	0.080
O(2)r_1	0.076	0.072	0.023	0.070	0.062	0.060
r_2	0.085	0.091	0.081	0.081	0.070	0.064
r_3	0.095	0.121	0.107	0.094	0.098	0.078
O(3)r_1	0.069	0.073	0.065	0.071	0.054	0.056
r_2	0.093	0.107	0.089	0.083	0.087	0.064
r_3	0.101	0.118	0.100	0.095	0.091	0.077

TABLE 6—*Continued*

	Ti_4O_7			$(Ti_{0.9975}V_{0.0025})_4O_7$		
	298°K	140°K	120°K	298°K	135°K	100°K
O(4)r_1	0.073	0.075	0.024	0.067	0.050	0.060
r_2	0.080	0.086	0.082	0.075	0.078	0.067
r_3	0.087	0.123	0.099	0.086	0.079	0.074
O(5)r_1	0.076	0.070	0.053	0.069	0.060	0.061
r_2	0.082	0.096	0.070	0.073	0.074	0.064
r_3	0.087	0.119	0.108	0.076	0.087	0.070
O(6)r_1	0.070	0.088	0.084	0.065	0.050	0.062
r_2	0.082	0.098	0.095	0.070	0.062	0.070
r_3	0.093	0.103	0.096	0.092	0.080	0.073
O(7)r_1	0.074	0.074	0.056	0.071	0.036	0.060
r_2	0.083	0.087	0.087	0.072	0.069	0.066
r_3	0.085	0.102	0.100	0.081	0.085	0.072
Mean value of RMS displacements of oxygen atoms						
	0.083	0.096	0.079	0.078	0.072	0.067
Standard deviation with respect to the RMSD mean value						
	0.008	0.018	0.026	0.010	0.017	0.007

[a] In this table the mean standard deviation for the titanium RMSD values are 0.001, 0.005, 0.006, 0.001, 0.001, and 0.001 Å, at 298, 140, 120, 298, 135, and 100°K, respectively. For the oxygen atoms they are 0.004, 0.011, 0.015, 0.002, 0.004, and 0.003 Å at the same temperatures.

TABLE VII

NORMALIZED Ti AND O CHARGES CALCULATED WITH THE ZACHARIASEN FORMULA IN THE O AND Ti COORDINATION POLYDRON, RESPECTIVELY

	Ti_4O_7[a]			$(Ti_{0.9975}V_{0.0025})_4O_7$		
	298°K	140°K	120°K	298°K	135°K	100°K
Ti(1)	3.482	3.427	3.015	3.473	3.423	3.038
Ti(2)	3.452	3.551	4.004	3.453	3.573	3.989
Ti(3)	3.598	3.478	3.085	3.602	3.498	3.094
Ti(4)	3.468	3.544	3.896	3.472	3.506	3.879
O(1)	2.053	2.056	2.132	2.057	2.064	2.073
O(2)	2.008	2.015	1.920	2.013	2.028	1.977
O(3)	2.114	2.104	2.024	2.110	2.092	2.070
O(4)	1.855	1.864	1.926	1.853	1.859	1.897
O(5)	1.989	2.000	2.061	1.993	2.005	2.022
O(6)	2.041	2.012	2.063	2.031	2.007	2.091
O(7)	1.940	1.949	1.874	1.943	1.945	1.870

[a] These values are calculated with Ti–O distances in (*6*).

Ti_2O_3	Rice and Robinson (*15*)
	$d(1) = 1.8285$
Ti_4O_7	Marezio *et al.* (*6*)
	$d(1) = 1.8300$
V doped Ti_4O_7	present work
	$d(1) = 1.8299$

Since the V doping was small, in the charge calculations it was not taken into account.

Discussion

On doping a crystal two effects must be taken into account in order to explain the lattice-parameter variations, one due to the different size of the dope and a second of electronic origin. In the present case the dope concentration is so small that the large variation observed (see Fig. 3) must be entirely due to an electronic effect. Furthermore, the lattice parameters of the two samples with different vanadium concentrations, 0.25 and 0.6% (*4*), are the same for both the metallic and intermediate phases. The low-temperature phase has not been observed for the 0.6% V-dope sample.

Two transitions are observed for the lattice parameters of the 0.25% V-doped sample, one at about 150°K and the second at 115°K on cooling and 130°K on warming. On cooling the unit-cell volume increases at both transitions of about the same percentage, ~0.35%. This behavior is quite different from that of pure Ti_4O_7 for which only the metal–semiconductor transition is accompanied by a lattice-parameter discontinuity and a volume increase of ~0.4% A hysteresis of about 15°K is observed for the lower transition, taking place in the V-doped sample. This is also observed in its electrical resistivity and specific heat. This clearly shows that a very small amount, 0.25% of vanadium, is enough to change the physical properties of Ti_4O_7. It should be noted that the *a* and *b* parameters increase at the lower transition, while the *c* parameter decreases. The first two parameters are contained in the $(1\bar{2}1)$ pseudorutile shear plane and form the two infinite directions of the rutile blocks, whereas *c* is almost along the finite direction.

As can be seen from Tables IV and V, where the Ti–O, O–O, and Ti–Ti interatomic distances are given, the structures of the three phases of $(Ti_{0.9975}V_{0.0025})_4O_7$ are almost identical to those of the corresponding phases of pure Ti_4O_7. The cationic charges given in Table VII show that at room temperature the distributions of charges along the 3113 and 4224 chains are 3.60–3.47–3.47–3.60 and 3.47–3.45–3.45–3.47, respectively. Therefore the charges are almost completely disordered except for those of the Ti(3) site, of which 60% seem to be occupied by Ti^{4+}. Exactly the same distribution was found for the metallic phase of pure Ti_4O_7, but a slightly different distribution was found for that of V_4O_7 at room temperature. In the intermediate phase of 0.25% V-doped Ti_4O_7 the charges have undergone a certain reordering. The distribution is 3.50–3.42–3.42–3.50 and 3.51–3.57–3.57–3.51 for the 3113 and 4224 chains, respectively. In the low-temperature phase the charges have completely ordered. The distribution in this phase is 3.09–3.04–3.04–3.09 for the 3113 chains and 3.88–3.99–3.99–3.88 for the 4224 chains. This corresponds to 93% of Ti^{3+} along the 3113 chains and an equal amount of Ti^{4+} along the 4224 chains. Along each chain the order is more complete in the sites inside the blocks, such as Ti(1) and Ti(2), than in sites at the edge, such as Ti(3) and Ti(4). The two octahedra around these cations share a face across the shear plane, and the disorder could be due to an electron transfer which takes place across this shared face.

At the lower phase the Ti–Ti pair bonds form in the $(Ti_{0.9975}V_{0.0025})_4O_7$ crystal in the same manner as in the pure Ti_4O_7. At room temperature the distances along the 3113 chains are Ti(3)–3.020–Ti(1)–2.891–Ti(1)–3.020–Ti(3), and they become 2.788–3.109–2.788 at 100°K, which clearly indicates the formation of the two covalent bonds between the $Ti^{3+}(3)$ and $Ti^{3+}(1)$ cations. The Ti–Ti distances along the 4224 chains also vary at

the lower transition; however, their variations tend to equalize the three distances. This is due to the fact that in the low-temperature phase these chains contain mainly cations, such as Ti^{4+}, with no *d* electron. The Ti(2) and Ti(4) sites zigzag along the 4224 chain, which is a consequence of the pairing taking place in the adjacent 3113 chain.

The intermediate phase of 0.25% V-doped Ti_4O_7 is characterized by a very small charge localization; however, no pair bonding can be deduced from the Ti–Ti distances. The same is true for the corresponding phase of pure Ti_4O_7. In order to reconcile the physical properties with the crystal structure for this latter compound, a disorder of the bonding pattern has been proposed. This speculation was corroborated by the anomalously large Debye–Waller factors of the cations, which are indicative of a disorder. It can be seen from Tables III and VI, where the thermal data for $(Ti_{0.9975}V_{0.0025})_4O_7$ are reported, that the intermediate phase of this compound also shows anomalously large thermal vibrations. However, on the average the anomalies are smaller in the 0.25% V-doped Ti_4O_7 crystal than in the pure Ti_4O_7 crystal. It should also be noted that in the low-temperature phase the cationic vibrations are quite anisotropic in pure Ti_4O_7, whereas in the 0.25% V-doped crystal they seem to be almost isotropic.

As has been stated above the main difference between the behavior of the pure Ti_4O_7 crystal and that of the 0.25% V-doped crystal is the discontinuity of the lattice parameters and unit-cell volume at the low transition for the 0.25% V-doped sample. These discontinuities are accompanied by a hysteresis of about 15°K. No transition is detected for pure Ti_4O_7. The volume variation is very anisotropic; in fact the *a* and *b* parameters increase on going from the intermediate to the low-temperature phase, whereas the *c* parameter decreases. The Ti–Ti distances along the 3113 and 4224 chains, which have a large component along the finite direction of the rutile direction, are smaller than those in pure Ti_4O_7. This indicates that the strengths of these bonds increase slightly in the V-doped sample.

In the metallic phase the vanadium cations are distributed in equal proportions over the 3113 and 4224 chains. In the low-temperature phase where the charges are localized, the vanadium cations would probably have either the 3^+ of the 4^+ charge. Therefore the incorporation of vanadium would give rise to four different patterns, which are schematized in Fig. 5.

- In scheme (a), a V^{4+} is supposed to be on a 3113 chain. Since V^{4+} is isoelectronic with Ti^{3+} it would probably form a normal bond.
- In scheme (b), a V^{3+} cations is supposed to be on a 3113 chain. This gives rise to a stronger bond between the V^{3+} and Ti^{3+} since an extra electron contributes to this bond. However, in this case the extra electron could go into an antibonding orbital and weaken the bond or it could go to the adjacent 4224 chain comprised of Ti^{4+} cations and create a Ti^{3+} on this chain.
- In scheme (c), a V^{4+} cation is supposed to be on a 4224 chain. This gives rise to an unpaired V^{4+}. This model is corroborated by EPR measurements (*16*) which indicate that a concentration of V^{4+} cations is present in the low-temperature phase. This concentration decreases with time after the quenching process, while the Ti^{3+} concentration increases. This process has been explained (*16*) as due to the establishment of thermodynamic equilibrium between schemes (c) and (c′). The X-ray diffraction experiments are done after the equilibrium has been reached, and therefore they see both the (c) and (c′) schemes.
- In scheme (d), a V^{3+} cation is supposed to be on a 4224 chain. This gives rise to a semipolar bond along the 4224 chain.

The extra pair bonds [schemes (c′) and (d)] on the "wrong" chains give rise to a distortion of the lattice because two bonds are

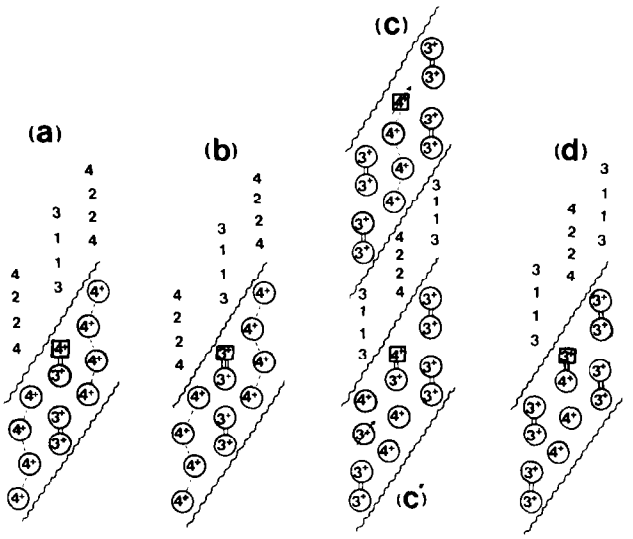

FIG. 5. Pseudorutile (110) sections of V-doped Ti_4O_7. The [001] axis is the vertical direction; the wavy lines represent the shear planes between each rutile block. The four schemes represent the different possibilities of the vanadium positions and charges at the low phase: (a) V^{4+} in 3113 chain, (b) V^{3+} in 3113 chain, (c) and (c') V^{4+} on 4224 chain, (d) V^{3+} on 4224 chain.

formed on adjacent chains. In order to obtain an equal distribution of the electrostatic forces the rutile blocks expand along the triclinic *a*- and *b*-axes and contract along the *c*-axis. On the contrary schemes (a) and (b) give rise to a distortion which is of a different type and much smaller.

In the intermediate phase only schemes (a) and (b) should exist because in this phase the pair occurs either on the 3113 or on the 4224 chains. Schemes (c') and (d) create a larger distortion, and thus they are less probable in a disordered phase. A large concentration of the vanadium cations on the "wrong" 4224 chains could be responsible for the suppression of the disorder–order transition. However it is surprising that one vanadium cation every 50 chains would stop the order process.

Acknowledgment

We would like to thank J. J. Since, S. Ahmed, and S. Lakkis of the Groupe des Transitions de Phases, CNRS, Grenoble, for their contribution to the crystal growing.

References

1. S. ANDERSSON AND L. JAHNBERG, *Ark. Kemi.* **21**, 413 (1963).
2. S. LAKKIS, C. SCHLENKER, B. K. CHAKRAVERTY, R. BUDER, AND M. MAREZIO, *Phys. Rev. B* **14**, 1429 (1976), and references cited therein.
3. J. L. HODEAU AND M. MAREZIO, *J. Solid State Chem.* **23**, 253 (1978), and references cited therein.
4. C. SCHLENKER, S. LAKKIS, S. AHMED, J. L. HODEAU, AND M. MAREZIO, *J. Phys. Chem. Solid State Phys.* **10**, L151 (1977).
5. S. AHMED, C. SCHLENKER, AND R. BUDER, *J. Magn. Mat.* **7**, 338 (1978).
6. M. MAREZIO, D. B. MCWHAN, P. D. DERNIER, AND J. P. REMEIKA, *J. Solid State Chem.* **6**, 213 (1973).
7. J. MERCIER AND S. LAKKIS, *J. Cryst. Growth* **20**, 195 (1973).
8. J. L. HODEAU, M. MAREZIO, C. SCHLENKER, R. BUDER, AND S. LAKKIS, *J. Appl. Crystallogr.* **9**, 391 (1976).
9. M. MAREZIO, P. D. DERNIER, D. B. MCWHAN, AND J. P. REMEIKA, *Mater. Res. Bull.* **5**, 1015 (1970).
10. P. A. DOYLE AND P. S. TURNER, *Acta Crystallogr. A* **24**, 390 (1968).
11. D. T. CROMER AND D. LIBERMAN, *J. Chem. Phys.* **53**, 1891 (1970).

12. W. H. ZACHARIASEN, private communication.
13. S. C. ABRAHAMS AND J. L. BERNSTEIN, *J. Chem. Phys.* **55**, 3206 (1971).
14. W. R. ROBINSON, *J. Solid State Chem.* **9**, 255 (1974).
15. C. E. RICE AND W. R. ROBINSON, *Acta Crystallogr. B* **33**, 1342 (1977).
16. C. SCHLENKER, B. K. CHAKRAVERTY, AND R. BUDER, "Proceedings, Int. Conf. Phys. Semic., Rome, 1976, p. 334."